Impact of Tortuosity on Charge-Carrier Transport in Organic Bulk Heterojunction Blends

Michael C. Heiber,[1,*] Klaus Kister,[2] Andreas Baumann,[3] Vladimir Dyakonov,[2,3]
Carsten Deibel,[4] and Thuc-Quyen Nguyen[1,†]

[1]*Center for Polymers and Organic Solids, University of California, Santa Barbara, California 93106, USA*
[2]*Experimental Physics VI, Julius-Maximilian University of Würzburg, 97074 Würzburg, Germany*
[3]*Bavarian Centre for Applied Energy Research (ZAE Bayern), 97074 Würzburg, Germany*
[4]*Institut für Physik, Technische Universität Chemnitz, 09126 Chemnitz, Germany*

(Received 10 April 2017; revised manuscript received 2 October 2017; published 22 November 2017)

The impact of the tortuosity of the charge-transport pathways through a bulk heterojunction film on the charge-carrier mobility is theoretically investigated using model morphologies and kinetic Monte Carlo simulations. The tortuosity descriptor provides a quantitative metric to characterize the quality of the charge-transport pathways, and model morphologies with controlled domain size and tortuosity are created using an anisotropic domain growth procedure. The tortuosity is found to be dependent on the anisotropy of the domain structure and is highly tunable. Time-of-flight charge-transport simulations on morphologies with a range of tortuosity values reveal that tortuosity can significantly reduce the magnitude of the mobility and the electric-field dependence relative to a neat material. These reductions are found to be further controlled by the energetic disorder and temperature. Most significantly, the sensitivity of the electric-field dependence to the tortuosity can explain the different experimental relationships previously reported, and exploiting this sensitivity could lead to simpler methods for characterizing and optimizing charge transport in organic solar cells.

DOI: 10.1103/PhysRevApplied.8.054043

I. INTRODUCTION

Extensive development efforts on organic photovoltaics (OPVs) over the last two decades have generated major performance improvements. To achieve high performance, most OPVs use a bulk heterojunction (BHJ) blend of electron-donating and electron-accepting materials to enhance the conversion of photogenerated excitons into free charge carriers. Because of the small exciton diffusion length in most organic semiconductors, optimized BHJ structures have nanoscale, donor-rich and acceptor-rich domains that form a complex interpenetrating network that enhances exciton harvesting, charge separation, and charge transport, while minimizing recombination losses. It has become very clear that morphological control is one of the most important issues for creating efficient OPVs [1], but the details about specifically which morphological features are needed and their precise roles are still being investigated.

It is well established that the charge-carrier mobilities should be high so that charge carriers are extracted from the active layer before recombination can occur [2–4], but a detailed understanding of the fundamental relationships between the BHJ morphology and the resulting mobilities is still needed. Ideally, charge carriers would have a direct pathway to their respective electrodes that is parallel to the electric-field vector, but real morphologies can have convoluted transport pathways that slow down charge extraction. In several BHJ blends, the electron and/or hole mobility can be significantly decreased compared to the neat material [3,5–9]. Whether this drop is due to disruptions in crystallinity or due to the formation of poor charge-transport pathways is not usually clear. However, Proctor *et al.* concluded that, in at least two small molecule-fullerene blends, poor domain connectivity can explain the reduced hole mobility [9], and Foster *et al.* also deduced that connectivity problems explain the low electron mobility in PTB7:PCBM blends [8]. Concerns about this issue were the major driving force for the proposed "ideal" vertically aligned pillar morphology that was heavily pursued a decade ago [10].

While it is challenging to experimentally characterize the charge-transport pathways in a BHJ morphology, transmission-electron-microscope (TEM) tomography techniques have been a powerful tool for imaging the complex three-dimensional structure [11–15]. Using these techniques, a number of studies have qualitatively assessed the transport pathways and have found that processing conditions can have a significant impact [14,16,17]. For a more quantitative analysis, Wodo *et al.* have utilized the tortuosity descriptor to characterize the transport pathways in model morphologies [18]. Tortuosity quantitatively indicates how convoluted a transport pathway is relative to the shortest straight path. Using this descriptor, Wodo *et al.* then showed how tortuosity histograms can be determined from TEM tomography measurements and demonstrated how processing conditions can impact the tortuosity [19]. The effect of tortuosity on transport has often been studied in

*heiber@mailaps.org
†quyen@chem.ucsb.edu

percolation theory and in the context of transport through porous media [20–22], but the concept has rarely been explored in the OPV field [17–19,23,24].

The complex morphology is also difficult to simulate with atomistic detail, so simplified models such as the Ising-based model are commonly used [24–26]. One of the few simulation techniques that is able to incorporate the nanoscale morphological details and simulate charge transport is the kinetic Monte Carlo (KMC) method. Using this technique, researchers have investigated a wide range of important fundamental structure-property relationships in OPVs [27–29]. With specific regard to charge transport, KMC simulations with model BHJ morphologies have revealed significantly lower mobilities than in a neat material due to the morphology [30–32]. Several studies have also shown that the electric-field dependence of the mobility changes from positive to negative when comparing neat and BHJ films [32–34].

Experimentally, in many amorphous molecularly doped polymers [35–40] and in neat organic semiconductors that are disordered [36,41–44] and even semicrystalline [45,46], a mobility with a positive field dependence that follows the Poole-Frenkel model has been regularly observed, as long as significant positional disorder is not present [37,47,48]. However, in BHJ blend films, a mobility with a negative field dependence has been frequently observed [49–56], while some blends still exhibit a positive field dependence [57–61] or even no field dependence [62,63]. While differences between mobility measurement techniques and conditions among these studies could play a role in explaining the differences in the observed field dependence, the previously discussed simulation results suggest that morphological details play an important and potentially dominant role. Overall, there is still an urgent need to understand how the details of the BHJ phase morphology affect charge transport.

In this study, we demonstrate the use of anisotropic interaction energies with the Ising-based morphology model to create well-controlled, model BHJ morphologies with charge-transport pathways that have varying degrees of tortuosity. Then, using KMC charge-transport simulations on these model morphologies and neat films, we show that the electric-field dependence of the charge-carrier mobility in a BHJ blend is highly affected by the tortuosity. This development can explain apparent discrepancies between a variety of different experimental and theoretical studies and illuminates an important fundamental physical structure–property relationship that could be used to accelerate materials optimization for organic solar cells.

II. METHODS

A. Morphology model

To probe how tortuosity affects charge transport and isolate tortuosity effects from other factors, we implement a simple, well-controlled Ising-based morphology model. In previous experimental work, Moon *et al.* have shown that in some materials, domains can be anisotropically oriented in the film, and they have shown that charge extraction is slower when domains are elongated in the plane of the film [64]. Drawing inspiration from this concept, we have extended the Ising_OPV v2.0 morphology model [65] by implementing controllable anisotropic phase separation in Ising_OPV v3.0 [66]. The standard Ising-based model uses an interaction energy (J) to modulate the driving force for phase separation [24], but by modifying the interaction energy in one direction, domain growth during phase separation becomes anisotropic.

To tune the tortuosity in a controlled manner, an additional directional dependent interaction energy (ΔJ_z) in the z direction is added to the interaction energy equation used in the bond formation algorithm [24]. As a result, the energy change for swapping two neighboring sites is

$$\Delta\epsilon = -\Delta N_1 J - \Delta N_2 \frac{J}{\sqrt{2}} - \Delta N_{1,z}\Delta J_z, \tag{1}$$

where ΔN_1 is the change in the number of total first-nearest-neighbor like-like bonds, ΔN_2 is the change in the number of total second-nearest-neighbor like-like bonds, and $\Delta N_{1,z}$ is the change in the number of first-nearest-neighbor like-like bonds in the z direction. The number of like-like bonds is the sum of donor-donor and acceptor-acceptor bonds. This additional interaction energy in the z direction causes preferential growth in the x-y plane, and so we define the anisotropic driving force

$$\Delta J_{xy} = -\Delta J_z. \tag{2}$$

With a positive value of ΔJ_{xy}, there is preferential domain growth in the x-y plane, and with a negative value, there is preferential domain growth in the z direction. To characterize the resulting anisotropy of the domain mesostructure, we define the domain anisotropy (γ)

$$\gamma = \frac{2\xi_z}{\xi_x + \xi_y}, \tag{3}$$

where ξ_x, ξ_y, and ξ_z are the correlation lengths in the x, y, and z directions, respectively.

All morphologies are created with a 50:50 blend ratio, and the duration of the phase-separation process is varied to obtain a range of domain sizes following previously developed methods [24,67]. The resulting morphologies consist of a bicontinuous, well-connected network of pure domains, and the pair-pair correlation method is used to characterize the average domain size (d) [24,68]. The characteristic tortuosity (τ) of each morphology is defined as the average geometric tortuosity [22].

$$\tau = \langle \tau_g \rangle = \frac{\langle L_g \rangle}{L}. \quad (4)$$

To calculate this descriptor, Dijkstra's algorithm is used to determine the shortest pathways through each phase from each corresponding point on the top of the lattice to the bottom (L_g) [69]. This shortest path through the film is then divided by the lattice height (L) to yield the geometric tortuosity for that specific pathway, and this is repeated to produce a tortuosity distribution. The tortuosity distribution is approximately Gaussian, and from it, the average tortuosity is determined. With a 50:50 blend ratio, the donor and acceptor phases have the same average tortuosity.

For the charge-transport simulations, seven morphology sets (MS1, MS2, MS3, MS4, MS5, MS6, MS7) are generated using the Ising_OPV v3.0 software tool [66]. For each set, 96 independent morphologies are generated on a lattice with final dimensions of $200 \times 200 \times 240$, which avoid finite lattice size effects. More detailed information about the morphology generation and characterization is shown in the Supplemental Material [70].

B. Charge transport

To determine the impact that the tortuosity has on charge transport, time-of-flight KMC simulations are performed on a 3D lattice with a thickness (L) of 240 sites and a lattice constant (a) of 1 nm. Energetic disorder is included using an uncorrelated Gaussian density of states (DOS) defined by a standard deviation (σ). Some materials have been argued to be best described by a correlated Gaussian disorder model, which explains the Poole-Frenkel behavior observed even at low electric-field strengths [71,72]. However, we assume that the fundamental effect of tortuosity on charge-transport behavior will be very similar regardless of whether the disorder is correlated or not. Simulations are done in the low-charge-carrier density regime ($1 \times 10^{-7}\ a^{-3} = 1 \times 10^{14}\ \mathrm{cm}^{-3}$) at which the mobility with a Gaussian DOS is independent of the carrier density [73–76]. Under these conditions, the charge carriers are sufficiently thermalized before extraction, and the natural logarithm of the zero-field mobility is proportional to $1/T^2$ as expected at equilibrium [76,77].

In each time-of-flight simulation, a single hole is randomly placed on a donor site at the top surface of the lattice and then allowed to undergo Miller-Abrahams hopping transport under the influence of an applied electric field (F) at a specified temperature (T), with the hopping rate defined [78]:

$$R_{ij} = \nu_0 \exp(-2\gamma d_{ij}) f_B(\Delta E_{ij}), \quad (5)$$

where ν_0 is the attempt to hop frequency, γ is the charge localization parameter, d_{ij} is the distance between sites, and

$$f_B(\Delta E_{ij}) = \begin{cases} \exp(-\Delta E_{ij}/kT) & \Delta E_{ij} > 0 \\ 1 & \Delta E_{ij} \le 0 \end{cases}. \quad (6)$$

ΔE_{ij} is the change in potential energy for the proposed charge hop,

$$\Delta E_{ij} = E_i - E_j + \Delta E_{C,ij} - F d_z, \quad (7)$$

where E_i and E_j are the initial and final site energies, $\Delta E_{C,ij}$ is the change in Coulomb potential that would occur for hopping from site i to site j, and d_z is the z-direction component of the hopping vector. However, in this study Coulomb interactions are not included since only one charge is simulated at a time.

Hole hopping is restricted to donor sites and is calculated for sites up to 3 nm away from the starting site. To simplify the simulations, image charge interactions with the electrodes are not included. Once the hole reaches the bottom surface, it is removed from the lattice, the transit time (t_{tr}) is recorded, and the entire process is repeated. After 20 charges are collected, the energetic disorder of the lattice is reassigned randomly from the Gaussian density-of-states distribution. This process is repeated for 1000 holes on each of the 96 morphologies in each morphology set, and the final mean mobility is determined based on the 96 000 total charge-transport runs. Additional KMC simulation details are provided in the Supplemental Material [70].

In organic semiconductors, it can be misleading to describe the charge-carrier mobility as a single characteristic average value due to a broad distribution of transport rates [79]. Because of a typically highly skewed distribution, the specific definition of the average is critical [80]. Many previous KMC charge-transport simulations calculate the mobility using the average transit time. However, with this method, even a small fraction of carriers with a very long transit time can have a major impact, causing the calculated mobility to greatly underestimate the transport velocity of the majority of the charge carriers. Furthermore, common experimental mobility measurement techniques that rely on a measurement of the current are more sensitive to the faster carriers, and a better alternative is to calculate the mean mobility using the average of the inverse of the transit time [80],

$$\mu_m = \frac{L}{F}\left\langle \frac{1}{t_{\mathrm{tr}}} \right\rangle. \quad (8)$$

The mean mobility represents the behavior of most charge carriers and can be more directly compared with experimental results.

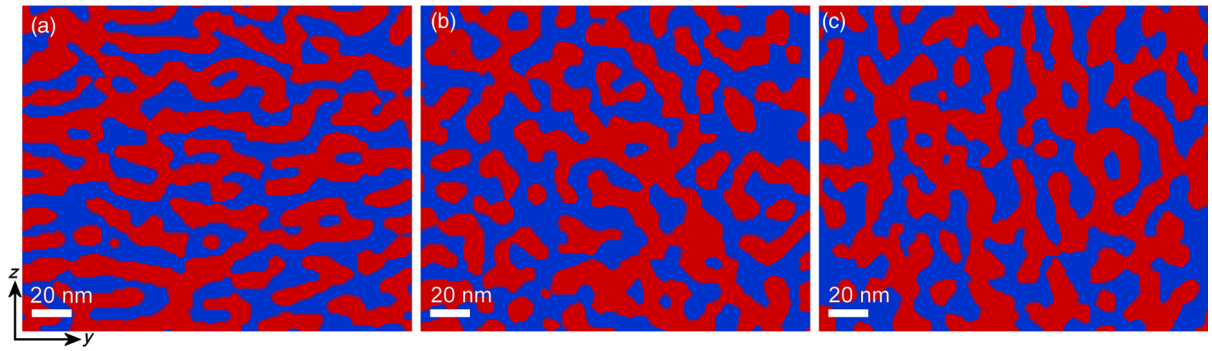

FIG. 1. Cross-sectional images (y-z plane) of morphologies with 8-nm average domain size. (a) an anisotropic morphology with horizontally elongated domains created with $\Delta J_{xy} = 0.1$ giving $\tau = 1.15$, (b) an isotropic morphology created with $\Delta J_{xy} = 0$ giving $\tau = 1.07$, and (c) an anisotropic morphology with vertically aligned domains created with $\Delta J_{xy} = -0.05$ giving $\tau = 1.05$.

III. RESULTS AND DISCUSSION

A. Morphology model

A wide range of tests are done to characterize the growth kinetics and resulting structure of the anisotropic bulk heterojunction morphologies. As a visual example of the resulting morphologies, Fig. 1 shows cross-sectional images of the y-z plane from individual morphologies created with varying ΔJ_{xy} values but with an equal domain size of 8 nm. Relative to the isotropic morphology shown in Fig. 1(b), Fig. 1(a) shows in-plane elongation of the domains in the y direction, and in Fig. 1(c), elongation can be seen in the out-of-plane, z direction. Despite the visual appearance of islands in the cross-sectional images, the phases are very well connected, and the vast majority of the apparent islands continue through the plane of the image and connect with the overall bicontinuous phase structure.

More quantitatively, Fig. 2 shows how the domain anisotropy evolves as the domains grow in size during the phase-separation process and how this anisotropy affects the tortuosity. A domain anisotropy value of 1 indicates an isotropic morphology, which has relatively direct charge-transport pathways and a relatively low tortuosity. With increased preference for domain growth in the x-y plane, the domain anisotropy values are less than one and the tortuosity increases significantly as the transport pathways become more convoluted. At a domain size of 8 nm, there is a relatively broad spread of tortuosity values depending on the anisotropic driving force value used, and these conditions are used to generate more complete morphology sets for charge-transport simulations. Several morphology sets are also constructed using a scaling technique [24] to yield domain sizes of 16 nm with the same tortuosity. Table I shows the important final characteristics of the seven morphology sets (MS1, MS2, MS3, MS4, MS5, MS6, MS7). The uncertainty values reported in the table represent the standard deviation of the characteristics determined for each of the 96 individual morphologies in each set. Additional characterization of these sets is shown in the Supplemental Material [70].

B. Charge transport

To provide a reference point for understanding the impact that the BHJ structure and tortuosity has on charge transport, we first simulate and analyze transport in a neat material. For transport in neat films, expanding on the traditional Gaussian disorder model [77], Novikov *et al.* showed that the electric-field dependence of the mobility can be described with a normalized unitless electric field [81]. Later, Pasveer *et al.* showed that the mobility can also be normalized to a unitless parameter [74]. In this normalized form, the mobility can be expressed as a function of the effective disorder ($\hat{\sigma}$), where $\hat{\sigma} = \sigma/kT$. Based on these concepts, we have performed a similar analysis. For

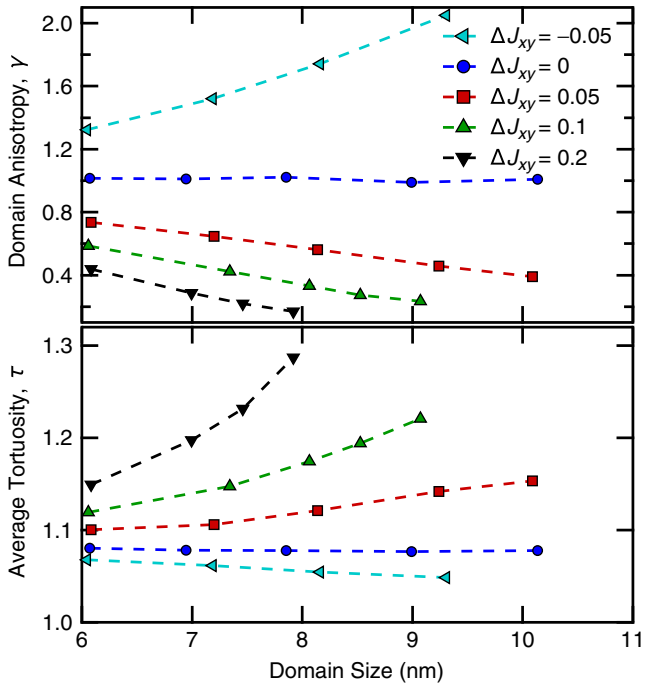

FIG. 2. (top) Domain anisotropy evolution as domains grow during phase separation and (bottom) the resulting average tortuosity of the charge-transport pathways.

TABLE I. Morphology set information.

Set	ΔJ_{xy}	Domain size, d (nm)	Tortuosity, τ
MS1	−0.05	8.02 ± 0.02	1.05 ± 0.01
MS2	0.05	8.00 ± 0.02	1.10 ± 0.01
MS3	0.10	8.06 ± 0.03	1.15 ± 0.02
MS4	0.20	7.92 ± 0.02	1.24 ± 0.03
MS5	−0.05	15.85 ± 0.08	1.05 ± 0.01
MS6	0.05	15.81 ± 0.09	1.11 ± 0.02
MS7	0.10	16.0 ± 0.1	1.15 ± 0.03

the neat film simulation results shown in Fig. 3 (left), the mobility in the intermediate, field-activated regime can be approximated as

$$\frac{\mu_{\text{neat}}}{\mu_0} = c_1 \exp\left[-c_2\hat{\sigma}^2\right] \exp\left[(c_3\hat{\sigma}^2 + c_4)\sqrt{\frac{F}{F_0}}\right], \quad (9)$$

where $\mu_0 = a^2\nu_0 e/\sigma$ and $F_0 = \sigma/ea$. When $(F/F_0)^{1/2} < 0.6$, the mobility begins to plateau as expected with an uncorrelated Gaussian DOS [48], and the mobility begins to saturate when $F > \sigma/ea$ [81]. The behavior in these regimes is not dominated by field-activated hopping and is therefore not well represented by Eq. (9). Detailed fitting and analysis results for the neat material simulations are shown in the Supplemental Material [70].

Moving on to the BHJ blends, the results shown in Fig. 3 demonstrate that this normalization scheme also works for describing the mobility in BHJ blends and that the mobility in a given blend still depends on the effective disorder. The closed symbols are from simulations with a fixed energetic disorder and varying temperature, and the open symbols are from simulations with a fixed temperature and varying energetic disorder. In all cases, both the open and closed symbols in Fig. 3 overlay each other, thereby validating the use of the effective disorder. After testing morphologies with 8- and 16-nm domains, we find little-to-no domain-size dependence. Instead, we find that the mobility is very sensitive to the tortuosity, exhibiting two distinct changes in the transport behavior. As tortuosity increases, the overall magnitude of the mobility is greatly reduced, and there is a dramatic decrease in the electric-field dependence. However, we emphasize that our results show that a negative field dependence is not an inherent property of BHJ blends, but instead depends on a combination of the tortuosity, energetic disorder, and temperature. This finding likely explains why both a positive and a negative field dependence have been observed in experimental studies on different BHJ blend systems [49–63].

To focus on the impact of the tortuosity apart from the details of the mobility behavior in the neat material, the deviation from the neat mobility can be described by adding two additional terms to Eq. (9),

$$\frac{\mu_{\text{BHJ}}}{\mu_0} = \frac{\mu_{\text{neat}}}{\mu_0} f(\hat{\sigma},\tau) \exp\left[g(\hat{\sigma},\tau)\sqrt{\frac{F}{F_0}}\right], \quad (10)$$

where $f(\hat{\sigma},\tau)$ represents the reduction in the magnitude of the zero-field mobility, and $g(\hat{\sigma},\tau)$ captures the change in the slope of the field dependence relative to the neat material. After fitting Eq. (10) to all blend simulations with varying tortuosity, energetic disorder, temperature, and domain size, Fig. 4 shows how f and g depend on the tortuosity and the effective disorder. We find that when the effective disorder is low, tortuosity can significantly reduce the zero-field mobility but has very little impact on the field dependence. Conversely, with larger effective disorder, where there is field-activated hopping, the tortuosity has almost no impact on the zero-field mobility and causes a strong reduction in the field dependence. More detailed

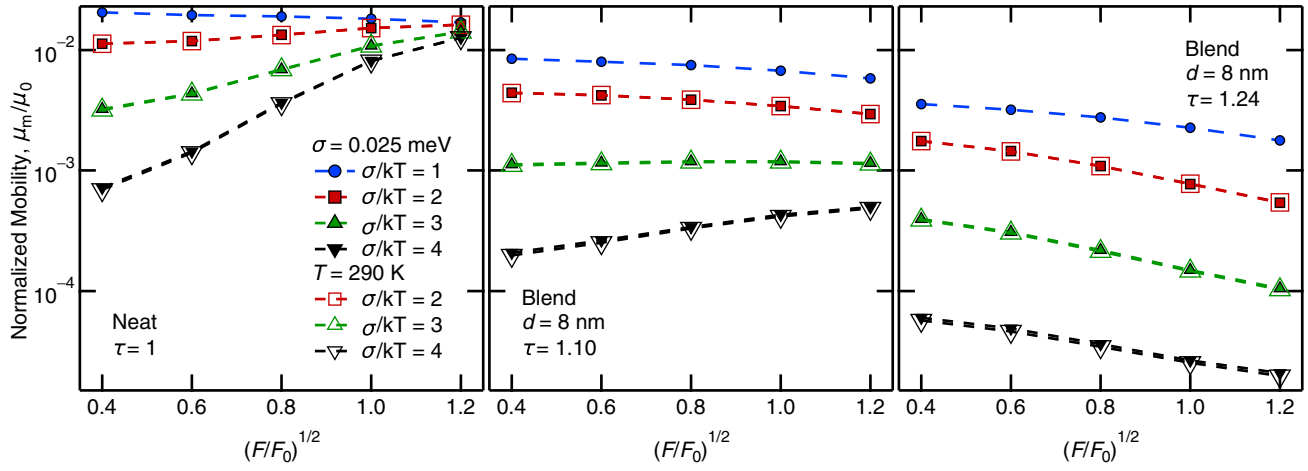

FIG. 3. Electric-field dependence of the normalized mobility in a neat film (left), a medium tortuosity blend (middle), and a high tortuosity blend (right) for different temperatures and energetic disorder values.

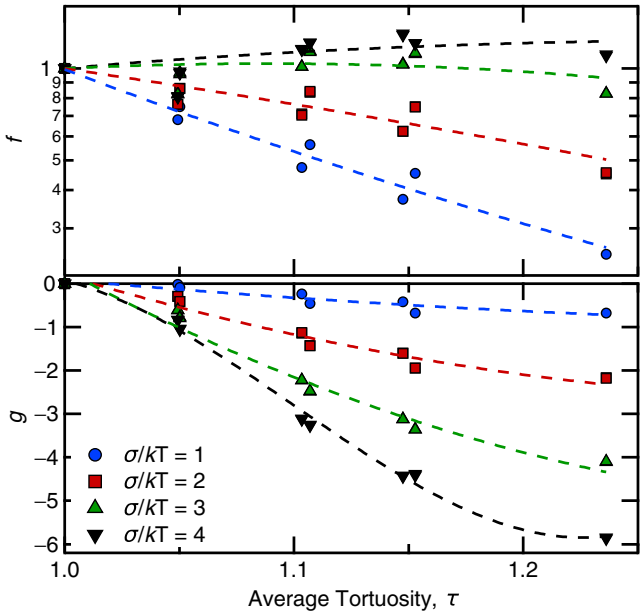

FIG. 4. Fit parameters quantifying the deviation in the mobility behavior from the neat film due to the tortuosity of the BHJ morphologies with dashed lines to guide the eye.

fitting results for both neat and blend films are shown in the Supplemental Material [70].

Overall, the largest impact of tortuosity is a major reduction in the electric-field dependence of the mobility. Similar to how positional disorder has been shown to reduce the field dependence in molecularly doped systems [37,47,48], convoluted charge-transport pathways force charges to move perpendicular to the electric-field vector in order to continue traveling through the film, which causes the mobility to decrease. While this general phenomenon has been explained before in the context of BHJ blends [32], we show here that this effect varies in magnitude depending on the tortuosity of the morphology.

Taking advantage of this phenomenon, we propose that a combination of electric-field and temperature-dependent mobility measurements could be used to answer several important questions relevant for optimizing BHJ blends for organic solar cells. By extrapolating field-dependent mobility measurements to zero field and then plotting the zero-field mobility as a function of the temperature, one could calculate the energetic disorder (σ) using Eq. (9). The zero-field mobility is only weakly affected by tortuosity, as evidenced by the small change in f values in Fig. 4 for realistic disorder values of $\sigma/kT > 2$, but strongly depends on the energetic disorder. Using the calculated energetic disorder (σ), one could then plot the normalized mobility (μ/μ_0) against the normalized field (F/F_0) similar to Fig. 3 and also calculate the effective disorder (σ/kT) for each temperature. From this normalized data set, first, one could identify whether energetic disorder or tortuosity is the dominant factor limiting the mobility. Films limited by energetic disorder should exhibit a positive field dependence at room temperature, while films limited by tortuosity should exhibit a negative field dependence that remains negative even at low temperatures. Second, one could use this procedure to compare films prepared using different fabrication conditions to distinguish how a particular processing method changes the energetic disorder and the tortuosity. Relative tortuosity changes between samples could be determined by comparing the field dependence of the normalized mobility from curves with equivalent effective disorder (σ/kT). As observed in Fig. 3, for a given effective disorder, the field dependence (slope) is highly sensitive to the tortuosity.

IV. CONCLUSIONS

Overall, given the strong impact that tortuosity has on the electric-field dependence of the charge-carrier mobility observed in our simulations, we predict that the tortuosity will be a dominant factor that modifies the field dependence in a BHJ film relative to the neat material. This can explain why experimental studies over the years have reported positive and negative field dependence in blends of different materials. Given this strong relationship and the major challenges in quantifying the tortuosity using three-dimensional imaging techniques, there is great potential to use detailed mobility measurements to probe the quality of the charge-transport pathways. Based on these theoretical results, we propose that a combination of field- and temperature-dependent mobility measurements could be used to provide a detailed assessment of the factors limiting the charge-transport in BHJ films. With this knowledge, one could make more precise recommendations for modifying the materials chemistry or film fabrication conditions in order to accelerate the development and optimization of materials for organic solar cells. In addition, the fundamental relationships between tortuosity and charge transport developed here may also be impactful in other applications where transport through nanostructured materials plays a key role.

ACKNOWLEDGMENTS

M. C. H and T.-Q. N. acknowledge funding by the Office of Naval Research (ONR) Grant No. N000141410076. A. B. is financed by the Bavarian Ministry of Economic Affairs and Media, Energy and Technology. C. D. acknowledges funding by Deutsche Forschungsgemeinschaft (DFG) Grant No. DE830/13-1. This work used the Extreme Science and Engineering Discovery Environment (XSEDE) for computing resources [82], which is supported by National Science Foundation Grant No. ACI-1053575, and M. C. H. acknowledges XSEDE computation allocation Grant No. TG-DMR150118.

[1] Nicholas E. Jackson, Brett M. Savoie, Tobin J. Marks, Lin X. Chen, and Mark A. Ratner, The next breakthrough for organic photovoltaics?, J. Phys. Chem. Lett. **6**, 77 (2015).

[2] Sarah R. Cowan, Natalie Banerji, Wei Lin Leong, and Alan J. Heeger, Charge formation, recombination, and sweep-out dynamics in organic solar cells, Adv. Funct. Mater. **22**, 1116 (2012).

[3] Christopher M. Proctor, John A. Love, and Thuc-Quyen Nguyen, Mobility guidelines for high fill factor solution-processed small molecule solar cells, Adv. Mater. **26**, 5957 (2014).

[4] Davide Bartesaghi, Irene Del Carmen Pérez, Juliane Kniepert, Steffen Roland, Mathieu Turbiez, Dieter Neher, and L. Jan Anton Koster, Competition between recombination and extraction of free charges determines the fill factor of organic solar cells, Nat. Commun. **6**, 7083 (2015).

[5] Valentin D. Mihailetchi, L. Jan Anton Koster, Paul W. M. Blom, Christian Melzer, Bert de Boer, Jeroen K. J. van Duren, and René A. J. Janssen, Compositional dependence of the performance of poly(p-phenylene vinylene): methanofullerene bulk-heterojunction solar cells, Adv. Funct. Mater. **15**, 795 (2005).

[6] Valentin D. Mihailetchi, Hangxing Xie, Bert de Boer, L. Jan Anton Koster, and Paul W. M. Blom, Charge transport and photocurrent generation in poly(3-hexylthiophene): methanofullerene bulk-heterojunction solar cells, Adv. Funct. Mater. **16**, 699 (2006).

[7] Jonathan A. Bartelt, Zach M. Beiley, Eric T. Hoke, William R. Mateker, Jessica D. Douglas, Brian A. Collins, John R. Tumbleston, Kenneth R. Graham, Aram Amassian, Harald Ade, Jean M. J. Fréchet, Michael F. Toney, and Michael D. McGehee, The importance of fullerene percolation in the mixed regions of polymer-fullerene bulk heterojunction solar cells, Adv. Energy Mater. **3**, 364 (2013).

[8] Samuel Foster, Florent Deledalle, Akiko Mitani, Toshio Kimura, Ki-Beom Kim, Takayuki Okachi, Thomas Kirchartz, Jun Oguma, Kunihito Miyake, James R. Durrant, Shuji Doi, and Jenny Nelson, Electron collection as a limit to polymer:PCBM solar cell efficiency: Effect of blend microstructure on carrier mobility and device performance in PTB7:PCBM, Adv. Energy Mater. **4**, 1400311 (2014).

[9] Christopher M. Proctor, Abhishek S. Kher, John A. Love, Ye Huang, Alexander Sharenko, Guillermo C. Bazan, and Thuc-Quyen Nguyen, Understanding charge transport in molecular blend films in terms of structural order and connectivity of conductive pathways, Adv. Energy Mater. **6**, 1502285 (2016).

[10] Kevin M. Coakley and Michael D. McGehee, Conjugated polymer photovoltaic cells, Chem. Mater. **16**, 4533 (2004).

[11] B. Viktor Andersson, Anna Herland, Sergej Masich, and Olle Inganäs, Imaging of the 3D nanostructure of a polymer solar cells by electron tomography, Nano Lett. **9**, 853 (2009).

[12] Svetlana S. van Bavel, Erwan Sourty, Gijsbertus de With, and Joachim Loos, Three-dimensional nanoscale organization of bulk heterojunction polymer solar cells, Nano Lett. **9**, 507 (2009).

[13] Andrew A. Herzing, Lee J. Richter, and Ian M. Anderson, 3D nanoscale characterization of thin-film organic photovoltaic device structures via spectroscopic contrast in the TEM, J. Phys. Chem. C **114**, 17501 (2010).

[14] Lawrence F. Drummy, Robert J. Davis, Diana L. Moore, Michael Durstock, Richard A. Vaia, and Julia W. P. Hsu, Molecular-scale and nanoscale morphology of P3HT: PCBM bulk heterojunctions: Energy-filtered TEM and low-dose HREM, Chem. Mater. **23**, 907 (2011).

[15] John D. Roehling, K. Joost Batenburg, F. Benjamin Swain, Adam J. Moulé, and Ilke Arslan, Three-dimensional concentration mapping of organic blends, Adv. Funct. Mater. **23**, 2115 (2013).

[16] Joo-Hyun Kim, Min Kim, Hiroshi Jinnai, Tae Joo Shin, Haena Kim, Jong Hwan Park, Sae Byeok Jo, and Kilwon Cho, Organic solar cells based on three-dimensionally percolated polythiophene nanowires with enhanced charge transport, ACS Appl. Mater. Interfaces **6**, 5640 (2014).

[17] Louis A. Perez, James T. Rogers, Michael A. Brady, Yanming Sun, Gregory C. Welch, Kristin Schmidt, Michael F. Toney, Hiroshi Jinnai, Alan J. Heeger, Michael L. Chabinyc, Guillermo C. Bazan, and Edward J. Kramer, The role of solvent additive processing in high performance small molecule solar cells, Chem. Mater. **26**, 6531 (2014).

[18] Olga Wodo, Srikanta Tirthapura, Sumit Chaudhary, and Baskar Ganapathysubramanian, Computational characterization of bulk heterojunction nanomorphology, J. Appl. Phys. **112**, 064316 (2012).

[19] Olga Wodo, John D. Roehling, Adam J. Moulé, and Baskar Ganapathysubramanian, Quantifying organic solar cell morphology: A computational study of three-dimensional maps, Energy Environ. Sci. **6**, 3060 (2013).

[20] M. Ben Clennell, Tortuosity: A guide through the maze, in *Developments in Petrophysics*, Special Publications Vol. 122, edited by M. A. Lovell and P. K. Harvey (Geological Society, London, 1997), p. 299.

[21] Allen Hunt, Robert Ewing, and Bezhad Ghanbarian, *Percolation theory for flow in porous media*, Lecture Notes in Physics Vol. 880 (Springer, Cham, Switzerland, 2014).

[22] Behzad Ghanbarian, Allen G. Hunt, Robert P. Ewing, and Muhammad Sahimi, Tortuosity in porous media: A critical review, Soil Sci. Soc. Am. J. **77**, 1461 (2013).

[23] Adam G. Gagorik, Jacob W. Mohin, Tomasz Kowalewski, and Geoffrey R. Hutchison, Monte Carlo simulations of charge transport in 2D organic photovoltaics, J. Phys. Chem. Lett. **4**, 36 (2013).

[24] Michael C. Heiber and Ali Dhinojwala, Efficient Generation of Model Bulk Heterojunction Morphologies for Organic Photovoltaic Device Modeling, Phys. Rev. Applied **2**, 014008 (2014).

[25] Peter K. Watkins, Alison B. Walker, and Geraldine L. B. Verschoor, Dynamical Monte Carlo modelling of organic solar cells: The dependence of internal quantum efficiency on morphology, Nano Lett. **5**, 1814 (2005).

[26] B. P. Lyons, N. Clarke, and C. Groves, The quantitative effect of surface wetting layers on the performance of organic bulk heterojunction photovoltaic devices, J. Phys. Chem. C **115**, 22572 (2011).

[27] Chris Groves, Developing understanding of organic photovoltaic devices: Monte Carlo models of geminate and non-geminate recombination, charge transport, and charge extraction, Energy Environ. Sci. **6**, 3202 (2013).

[28] Michael C. Heiber, Christoph Baumbach, Vladimir Dyakonov, and Carsten Deibel, Encounter-Limited Charge-Carrier Recombination in Phase-Separated Organic Semiconductor Blends, Phys. Rev. Lett. **114**, 136602 (2015).

[29] Michael C. Heiber, Thuc-Quyen Nguyen, and Carsten Deibel, Charge carrier concentration dependence of encounter-limited bimolecular recombination in phase-separated organic semiconductor blends, Phys. Rev. B **93**, 205204 (2016).

[30] Jarvist M. Frost, Fabien Cheynis, Sachetan M. Tuladhar, and Jenny Nelson, Influence of polymer-blend morphology on charge transport and photocurrent generation in donor-acceptor polymer blends, Nano Lett. **6**, 1674 (2006).

[31] C. Groves, L. J. A. Koster, and N. C. Greenham, The effect of morphology upon mobility: Implications for bulk heterojunction solar cells with nonuniform blend morphology, J. Appl. Phys. **105**, 094510 (2009).

[32] L. J. A. Koster, Charge carrier mobility in disordered organic blends for photovoltaics, Phys. Rev. B **81**, 205318 (2010).

[33] Cristiano F. Woellner, Zi Li, José A. Freire, Gang Lu, and Thuc-Quyen Nguyen, Charge carrier moblity in a two-phase disordered organic system in the low-carrier concentration regime, Phys. Rev. B **88**, 125311 (2013).

[34] Cristiano F. Woellner and José A. Freire, Impact of the intermixed phase and the channel network on the carrier mobility of nanostructured solar cells, J. Chem. Phys. **144**, 084119 (2016).

[35] L. B. Schein, A. Peled, and D. Glatz, The electric field dependence of the mobility in molecularly doped polymers, J. Appl. Phys. **66**, 686 (1989).

[36] P. M. Borsenberger, L. Pautmeier, and H. Bässler, Charge transport in disordered molecular solids, J. Chem. Phys. **94**, 5447 (1991).

[37] P. M. Borsenberger, E. H. Magin, M. van der Auweraer, and F. C. de Schryver, The role of disorder on charge transport in molecularly doped polymers and related materials, Phys. Status Solidi A **140**, 9 (1993).

[38] Paul M. Borsenberger and David S. Weiss, *Organic Photoreceptors for Imaging Systems*, Optical Science and Engineering (Marcel Dekker, New York, 1993).

[39] David H. Dunlap, Explanation for the $\sqrt{E}$-dependent mobilities of charge transport in molecularly doped polymers, Phys. Rev. B **52**, 939 (1995).

[40] David H. Dunlap, P. E. Parris, and V. M. Kenkre, Charge-Dipole Model for the Universal Field Dependence of Mobilities in Molecularly Doped Polymers, Phys. Rev. Lett. **77**, 542 (1996).

[41] Damodar M. Pai, Transient photoconductivity in poly(N-vinylcarbazole), J. Chem. Phys. **52**, 2285 (1970).

[42] P. M. Borsenberger and John J. Fitzgerald, Effects of dipole moment on charge transport in disordered molecular solids, J. Phys. Chem. **97**, 4815 (1993).

[43] Z. G. Yu, D. L. Smith, A. Saxena, R. L. Martin, and A. R. Bishop, Molecular geometry fluctuations and field-dependent mobility in conjugated polymers, Phys. Rev. B **63**, 085202 (2001).

[44] Sebastian T. Hoffmann, Frank Jaiser, Anna Hayer, Heinz Bässler, Thomas Unger, Stavros Athanasopoulos, Dieter Neher, and Anna Köhler, How do disorder, reorganization, and localization influence the hole mobility in conjugated copolymers?, J. Am. Chem. Soc. **135**, 1772 (2013).

[45] Attila J. Mozer, Niyazi Serdar Sariciftci, Almantas Pivrikas, Ronald Österbacka, Gytis Juška, Lutz Brassat, and Heinz Bässler, Charge carrier mobility in regioregular poly(3-hexylthiophene) probed by transient conductivity techniques: A comparative study, Phys. Rev. B **71**, 035214 (2005).

[46] Liang Wang, Daniel Fine, Debarshi Basu, and Ananth Dodabalapur, Electric-field-dependent charge transport in organic thin-film transistors, J. Appl. Phys. **101**, 054515 (2007).

[47] L. Pautmeier, R. Richert, and H. Bässler, Poole-Frenkel behavior of charge transport in organic solids with off-diagonal disorder studied by Monte Carlo simulation, Synth. Met. **37**, 271 (1990).

[48] I. I. Fishchuk, A. Kadashchuk, H. Bässler, and M. Abkowitz, Low-field charge-carrier hopping transport in energetically and positionally disordered organic materials, Phys. Rev. B **70**, 245212 (2004).

[49] Christopher R. McNeill and Neil C. Greenham, Charge transport dynamics of polymer solar cells under operating conditions: Influence of trap filling, Appl. Phys. Lett. **93**, 203310 (2008).

[50] Steve Albrecht, Wolfram Schindler, Jona Kurpiers, Juliane Kniepert, James C. Blakesley, Ines Dumsch, Sybille Allard, Konstantinos Fostiropoulos, Ullrich Scherf, and Dieter Neher, On the field dependence of free charge carrier generation and recombination in blends of PCPDTBT/$PC_{70}BM$: Influence of solvent additives, J. Phys. Chem. Lett. **3**, 640 (2012).

[51] Steve Albrecht, Silvia Janietz, Wolfram Schindler, Johannes Frisch, Jona Kurpiers, Juliane Kniepert, Sahika Inal, Patrick Pingel, Konstantinos Fostiropoulos, Norbert Koch, and Dieter Neher, Fluorinated copolymer PCPDTBT with enhanced open-circuit voltage and reduced recombination for highly efficient polymer solar cells, J. Am. Chem. Soc. **134**, 14932 (2012).

[52] Bingyuan Huang, Jojo A. Amonoo, Anton Li, X. Chelsea Chen, and Peter F. Green, Role of domain size and phase purity on charge carrier density, mobility, and recombination in poly(3-hexylthiophene):phenyl-C61-butyric acid methyl ester devices, J. Phys. Chem. C **118**, 3968 (2014).

[53] Wentao Li, Steve Albrecht, Liqiang Yang, Steffen Roland, John R. Tumbleston, Terry McAfee, Liang Yan, Mary Allison Kelly, Harald Ade, Dieter Neher, and Wei You, Mobility-controlled performance of thick solar cells based on fluorinated copolymers, J. Am. Chem. Soc. **136**, 15566 (2014).

[54] Christopher M. Proctor, Steve Albrecht, Martijn Kuik, Dieter Neher, and Thuc-Quyen Nguyen, Overcoming geminate recombination and enhancing extraction in solution-processed small molecule solar cells, Adv. Energy Mater. **4**, 1400230 (2014).

[55] Benjamin Bouthinon, Raphaël Clerc, Jérôme Vaillant, Jean-Marie Verilhac, Jérôme Faure-Vincent, David Djurado, Irina Ionica, Gabriel Man, Antoine Gras, Georges Pananakakis, Romain Gwoziecki, and Antoine Kahn, Impact of blend morphology on interface state recombination in bulk

heterojunction organic solar cells, Adv. Funct. Mater. **25**, 1090 (2015).

[56] Jiajun Peng, Yani Chen, Xiaohan Wu, Qian Zhang, Bin Kan, Xiaoqing Chen, Yongsheng Chen, Jia Huang, and Ziqi Liang, Correlating molecular structures with transport dynamics in high-efficiency small-molecule organic photovoltaics, ACS Appl. Mater. Interfaces **7**, 13137 (2015).

[57] Christian Melzer, Erik J. Koop, Valentin D. Mihailetchi, and Paul W. M. Blom, Hole transport in poly(phenylene vinylene)/methanofullerene bulk-heterojunction solar cells, Adv. Funct. Mater. **14**, 865 (2004).

[58] Attila J. Mozer, G. Dennler, N. S. Sariciftci, M. Westerling, A. Pivrikas, Ronald Österbacka, and Gytis Juška, Time-dependent mobility and recombination of the photoinduced charge carriers in conjugated polymer/fullerene bulk heterojunction solar cells, Phys. Rev. B **72**, 035217 (2005).

[59] Anthony J. Morfa, Alexandre M. Nardes, Sean E. Shaheen, Nikos Kopidakis, and Jao van de Lagemaat, Time-of-flight studies of electron-collection kinetics in polymer:fullerene bulk-heterojunction solar cells, Adv. Funct. Mater. **21**, 2580 (2011).

[60] Tracey M. Clarke, Jeff Peet, Andrew Nattestad, Nicolas Drolet, Gilles Dennler, Christoph Lungenschmied, Mario Leclerc, and Attila J. Mozer, Charge carrier mobility, bimolecular recombination and trapping in polycarbazole copolymer:fullerene (PCDTBT:PCBM) bulk heterojunction solar cells, Org. Electron. **13**, 2639 (2012).

[61] Johannes Widmer, Janine Fischer, Wolfgang Tress, Karl Leo, and Moritz Riede, Electric potential mapping by thickness variation: A new method for model-free mobility determination in organic semiconductor thin films, Org. Electron. **14**, 3460 (2013).

[62] Bronson Philippa, Martin Stolterfoht, Paul L. Burn, Gytis Juška, Paul Meredith, Ronald D. White, and Almantas Pivrikas, The impact of hot charge carrier mobility on photocurrent losses in polymer-based solar cells, Sci. Rep. **4**, 5695 (2014).

[63] Juliane Kniepert, Ilja Lange, Jan Heidbrink, Jona Kurpiers, Thomas J. K. Brenner, L. Jan Anton Koster, and Dieter Neher, Effect of solvent additive on generation, recombination, and extraction in PTB7:PCBM solar cells: A conclusive experimental and numerical simulation study, J. Phys. Chem. C **119**, 8310 (2015).

[64] Ji Sun Moon, Jang Jo, and Alan J. Heeger, Nanomorphology of PCDTBT:$PC_{70}BM$ bulk heterojunction solar cells, Adv. Energy Mater. **2**, 304 (2012).

[65] Michael C. Heiber, Ising_OPV v2.0, https://github.com/MikeHeiber/Ising_OPV, 2015.

[66] Michael C. Heiber, Ising_OPV v3.0, https://github.com/MikeHeiber/Ising_OPV, 2016.

[67] Michael C. Heiber and Ali Dhinojwala, Erratum: Efficient Generation of Model Bulk Heterojunction Morphologies for Organic Photovoltaic Device Modeling [Phys. Rev. Applied 2, 014008 (2014)] Phys. Rev. Applied **8**, 019902(E) (2017).

[68] Benjamin P. Lyons, Nigel Clarke, and Chris Groves, The relative importance of domain size, domain purity and domain interfaces to the performance of bulk-heterojunction organic photovoltaics, Energy Environ. Sci. **5**, 7657 (2012).

[69] Edsger W. Dijkstra, A note on two problems in connexion with graphs, Numer. Math. **1**, 269 (1959).

[70] See Supplemental Material at http://link.aps.org/supplemental/10.1103/PhysRevApplied.8.054043 for further simulation details and supplemental results.

[71] Yu. N. Gartstein and E. M. Conwell, High-field hopping mobility in molecular systems with spatially correlated energetic disorder, Chem. Phys. Lett. **245**, 351 (1995).

[72] P. E. Parris, V. M. Kenkre, and D. H. Dunlap, Nature of Charge Carriers in Disordered Molecular Solids: Are Polarons Compatible with Observations?, Phys. Rev. Lett. **87**, 126601 (2001).

[73] C. Tanase, E. J. Meijer, P. W. M. Blom, and D. M. de Leeuw, Unification of the Hole Transport in Polymeric Field-Effect Transistors and Light-Emitting Diodes, Phys. Rev. Lett. **91**, 216601 (2003).

[74] W. F. Pasveer, J. Cottaar, C. Tanase, R. Coehoorn, P. A. Bobbert, P. W. M. Blom, D. M. de Leeuw, and M. A. J. Michels, Unified Description of Charge-Carrier Mobilities in Disordered Semiconducting Polymers, Phys. Rev. Lett. **94**, 206601 (2005).

[75] J. O. Oelerich, D. Huemmer, and S. D. Baranovskii, How to Find Out the Density of States in Disordered Organic Semiconductors, Phys. Rev. Lett. **108**, 226403 (2012).

[76] S. D. Baranovskii, Theoretical description of charge transport in disordered organic semiconductors, Phys. Status Solidi B **251**, 487 (2014).

[77] H. Bässler, Charge transport in disordered organic photoconductors, Phys. Status Solidi B **175**, 15 (1993).

[78] Allen Miller and Elihu Abrahams, Impurity conduction at low concentrations, Phys. Rev. **120**, 745 (1960).

[79] Jason Seifter, Yanming Sun, Hyosung Choi, Byoung Hoon Lee, Thanh Luan Nguyen, Han Young Woo, and Alan J. Heeger, Measurement of the charge carrier mobility distribution in bulk heterojunction solar cells, Adv. Mater. **27**, 4989 (2015).

[80] Jens Lorrmann, Manuel Ruf, David Vocke, Vladimir Dyakonov, and Carsten Deibel, Distribution of charge carrier transport properties in organic semiconductors with gaussian disorder, J. Appl. Phys. **115**, 183702 (2014).

[81] S. V. Novikov, D. H. Dunlap, V. M. Kenkre, P. E. Parris, and A. V. Vannikov, Essential Role of Correlations in Governing Charge Transport in Disordered Organic Materials, Phys. Rev. Lett. **81**, 4472 (1998).

[82] John Towns, Timothy Cockerill, Maytal Dahan, Ian Foster, Kelly Gaither, Andrew Grimshaw, Victor Hazlewood, Scroot Lathrop, Dave Lifka, Gregory D. Peterson, Ralph Roskies, J. Ray Scott, and Nancy Wilkins-Diehr, XSEDE: Accelerating scientific discovery, Comput. Sci. Eng. **16**, 62 (2014).